Diffusive mobility of fractal aggregates over the entire knudsen number range

G. M. Wang and C. M. Sorensen
Department of Physics and Program for Complex Fluid Flows, Cardwell Hall, Kansas State University, Manhattan, Kansas 66506
(Received 24 March 1999)

We determine the effective mobility radius for fractal aggregate particles. Our method is to use static light scattering to measure the radius of gyration R_g of the aggregates, and dynamic light scattering to measure the diffusion coefficient hence the mobility radius R_m. The range of our results can be specified by the Knudsen number Kn, which is the mean free path of the medium molecules divided by the radius of the aggregate. Our results apply to the entire range of Kn from the continuum limit (Kn=0) to the free molecular limit (Kn $\gg 1$). In the continuum regime we find $R_m/R_g = 0.97 \pm 0.05$ when the aggregate fractal dimension is $D_f \simeq 2.15$, and 0.70 ± 0.05 when $D_f \simeq 1.75$. The latter result is independent of Kn for Kn$\lesssim 1.3$. The free molecular mobility goes as $R_m = aN^{0.44 \pm 0.03}$, where a is the monomer radius and N is the number of monomers per aggregate. Since $R_g \sim aN^{1/D_f}$, R_m/R_g is not a constant when Kn is large. We find for all Kn that the functionality of R_m/R_g must always begin with the correct $N \to 1$ limit, and this affects experimental observation.
[S1063-651X(99)00409-2]

PACS number(s): 82.70.−y, 05.40.−a, 36.20.−r

I. INTRODUCTION

Aerosols and colloids are important and common in both our natural and technical environments. The particles in these systems can combine to form random aggregates which are quantitively described as fractals [1–3]. Fractals are scale invariant objects that obey the relation [4]

$$N = k_0 \left(\frac{R_g}{a} \right)^{D_f}, \tag{1}$$

where N is the number of primary particles or monomers in the aggregate, R_g is the radius of gyration of the aggregate, a is the monomer radius, k_0 is a constant of order unity, and D_f is the fractal dimension. It is the scaling $N \propto R_g^{D_f}$ and the quantitative specification of D_f that make the fractal description viable.

Given the importance of aerosols and colloids, we desire to understand the physical properties of the aggregates. The fractal description of the static structure provides a quantitative basis for understanding these properties. The work presented here studies the diffusive transport of fractal aggregates in aerosols and colloids. The essence of the diffusive transport problem is to describe quantitatively the mobility radius of the aggregate, R_m. This is the radius of a solid sphere that has the same mobility as that of the aggregate. This problem has been addressed by many workers [5–17], some of whom predate the fractal concept. Significant work in the fractal era includes that of Wiltzius [9], who studied colloids of reaction limited cluster aggregates (RLCA) with $D_f \simeq 2.1$. Using static light scattering (SLS) to measure R_g and D_f, and dynamic light scattering (DLS) to measure the diffusion coefficient and hence the mobility radius R_m, he found $R_m \propto R_g$. Reanalysis of his data to include the effects of aggregate polydispersity concluded $R_m/R_g = 0.98$ [10]. Schmidt-Ott [12] used electrostatic classifiers to measure the drag force and hence R_m of silver aggregates in an aerosol before and after sintering to dense spheres. Our reanalysis of his data (below) shows that $R_m \propto N^{0.46}$, not N^{1/D_f} as implied by $R_m \propto R_g$. This may not be surprising since colloids and aerosols differ in the Knudsen number Kn, which equals the mean free path of the medium molecules divided by the particle radius. For the colloids Kn ~ 0, whereas in aerosols typically Kn > 0. Rogak, Flagan, and Nguyen [15] also studied the mobility of aerosol fractal aggregates with classifiers and found $R_m \propto R_g^{0.79}$ which for $D_f \simeq 1.75$ is equivalent to $R_m \propto N^{0.44}$. Cai and Sorensen [16] used SLS and DLS measurements on flame soot fractal aggregates, and found $R_m \propto N^{0.43}$ for $D_f = 1.79$. Their Knudsen number range was $6.7 <$ Kn < 22. These aerosol results have been explained in terms of the drag force being proportional to the two-dimensional projectional area of the aggregate [16]. This projectional area description becomes necessary when Kn is large.

Despite the excellent work mentioned above, gaps exist in our description of fractal aggregate diffusive mobility. For the colloidal, Kn~ 0 regime, only Wiltzius' data for $D_f \simeq 2.1$ exist. No work describes the diffusive transport of the important class of diffusion limited cluster aggregates (DLCA) which have $D_f \simeq 1.8$. Since aggregates are ''transparent'' for $D_f < 2$ and ''opaque'' for $D_f > 2$, the difference between RLCA and DLCA may be significant. The region of intermediate Kn is largely unexplored and we will see below that the similar functional dependencies for the three aerosol systems described above may be a coincidence. Because of this, more data are needed at intermediate Kn for clusters of more than just a few monomers.

The purpose of this paper is to fill in these gaps. We study with DLS and SLS both DLCA and RLCA colloids and a DLCA aerosol. The Knudsen number range for the aerosol is Kn=0.03–1.3. At the end, we combine our results with previous work to give a rather complete empirical description of diffusive transport of fractal aggregates.

II. BACKGROUND OF STATIC AND DYNAMIC LIGHT SCATTERING

For the convenience of description, the following terminologies and notations are adopted in this paper. R_m and R_g

represent the mobility radius and the radius of gyration for a single aggregate of N monomers, and $\langle R_m \rangle$ and $\langle R_g \rangle$ denote the experimentally measured values which are averages over the cluster size distribution. $R_{m,0}$ and $R_{g,0}$ will be used to describe the mobility radius and the radius of gyration of the mean size of the distribution for the polydispersed aggregates. Apparently, if the aggregates are monodispersed, then $R_m = \langle R_m \rangle = R_{m,0}$ and $R_g = \langle R_g \rangle = R_{g,0}$. Since static and dynamic light scattering are the main techniques used in this research, a brief summary of these methods is outlined below.

A. Static light scattering (SLS)

The light intensity scattered by a system of aggregates, $I(q)$, is described by [18]

$$I(q) = cI_0 nN^2 \sigma^m S(q), \tag{2}$$

where c is a calibration constant, and I_0, n, σ^m, and S(q) are the incident light intensity, aggregate number density (assumed for now monodisperse), monomer scattering cross section, and the structure factor of the aggregate, respectively. Also in Eq. (2) we show the magnitude of the scattering wave vector,

$$q = 4\pi\lambda^{-1} \sin(\theta/2), \tag{3}$$

where λ is the wavelength of the incident light, and θ is the scattering angle.

Based on the value of qR_g, scattering can be discussed in terms of scattering regimes: $qR_g \ll 1$, the Rayleigh regime; $qR_g \leqslant 1$, the Guinier regime; and $qR_g \gg 1$, the power-law regime.

In the Rayleigh regime $S(q) = 1$, so Eq. (2) simply becomes

$$I(0) = cI_0 nN^2 \sigma^m. \tag{4}$$

Since $n_0 = nN$ is the total number of monomers per unit volume, which ideally is conserved during aggregation, Eq. (4) indicates that $I(q) \propto nN^2 = n_0 N$. This displays the Tyndall effect, which means that as the ensemble of clusters aggregates, the increasing N will cause the system to scatter more light.

In the Guinier regime, $S(q) \simeq 1 - \frac{1}{3} q^2 R_g^2$. Thus, for a given aggregate, Eq. (2) becomes

$$\frac{I(0)}{I(q)} \simeq \left(1 + \frac{1}{3} q^2 R_g^2 \right). \tag{5}$$

Equation (5) shows that a plot of $I(0)/I(q)$ vs q^2 should be linear with a slope of $\frac{1}{3} R_g^2$; hence R_g can be measured.

In the power-law regime, $qR_g \gg 1$, and then [18,19]

$$S(q) = CC_p (qR_g)^{-D_f}. \tag{6}$$

In Eq. (6), C is a constant dependent on the form of the single cluster structure factor, typically $C = 1$, and C_p is a constant dependent on the size distribution of the aggregates [19]. Substitution of Eqs. (1) and (6) into Eq. (2) yields

$$I(q) = cI_o n_o \sigma_m C_p k_o (aq)^{-D_f}. \tag{7}$$

By Eq. (7), a log-log plot of $I(q)$ vs q yields a line with slope $-D_f$.

B. Dynamic light scattering (DLS)

Dynamic light scattering [20] measures the scattered light intensity autocorrelation function, $C(t) = \langle I(t) I(0) \rangle$, as a function of lag time t. In general, this autocorrelation decays exponentially with lag time due to diffusive motion of the aggregate, $C(t) = B_0 + B_1 e^{-t/\tau_c}$, where B_0 is a background signal, B_1 is a constant, and τ_c is the correlation time. Fitting to the autocorrelation curve will yield τ_c, which is linked to the diffusion coefficient D of the aggregate by

$$\tau_c = (2q^2 D)^{-1}. \tag{8}$$

Diffusion and drag are intimately tied together by the Einstein relation

$$D = \frac{k_B T}{f}, \tag{9}$$

where $k_B T$ is the thermal energy (k_B is Boltzmann's constant), and f is the coefficient of the drag force on the aggregate.

Whereas the thermal energy is universal, the drag force depends on the kinetic regime of the aggregate. For a spherical particle with radius R, the coefficient of the drag force in the continuum regime ($\mathrm{Kn} \ll 1$) is given by the well-known Stokes equation

$$f = 6\pi\eta R, \tag{10}$$

where η is viscosity of the medium. In the other limit, the free molecular regime ($\mathrm{Kn} \gg 1$), this coefficient is given by Epstein's equation [21]

$$f = \frac{8}{3} R^2 \rho \left(\frac{2\pi k_B T}{m} \right)^{1/2} \left(1 + \frac{\beta\pi}{8} \right), \tag{11}$$

where ρ is mass density of medium, m is the mean mass of the medium molecules, and β is the accommodation coefficient ($0 < \beta < 1$). In the transition regime ($\mathrm{Kn} \sim 1$), no theory gives f, but there is an empirical equation

$$f = \frac{6\pi\eta R}{C(\mathrm{Kn})}, \tag{12}$$

where $C(\mathrm{Kn})$ is Cunningham correction factor and is given [21] by

$$C(\mathrm{Kn}) = 1 + \mathrm{Kn}\,(C_1 + C_2 e^{-C_3/\mathrm{Kn}}) \tag{13}$$

with $C_1 = 1.257$, $C_2 = 0.4$, and $C_3 = 1.1$.

Fractal aggregates are ramified and do not have a spherical shape. As a result, any attempt to apply Eq. (10) through Eq. (13) to aggregates encounters the problem of what is meant by R. This problem can be approached by defining an effective mobility radius R_m for aggregates, so that the above equations are still valid for aggregates if one replaces R with R_m. Under this definition, the following equations will be used when calculating the coefficient of drag force for aggregates regardless of morphology:

FIG. 1. TEM image of a fresh TiO_2 aerosol particle.

$$f = 6\pi\eta R_m, \quad \mathrm{Kn} \ll 1, \tag{14}$$

$$f = \frac{6\pi\eta R_m}{C(\mathrm{Kn})}, \quad \mathrm{Kn} \sim 1, \tag{15}$$

$$f = \frac{8}{3} R_m^2 \rho \left(\frac{2\pi k_B T}{m}\right)^{1/2} \left(1 + \frac{\beta\pi}{8}\right), \quad \mathrm{Kn} \gg 1. \tag{16}$$

The purpose of this work is to determine the behavior of R_m for fractal aggregates throughout the entire Kn range.

III. EXPERIMENTAL METHOD

The TiO_2 aerosol was generated by thermal decomposition of titanium tetraisopropoxide (TTIP), similar to the method reported by Okuyama *et al.* [22]. TTIP vapor was generated by heating liquid TTIP to temperatures around 80 °C and the vapor was carried into a half meter long tube furnace by dry N_2 gas with a flow rate of 0.5 liter per minute. The furnace was set to a temperature of ~400 °C. The decomposition of TTIP vapor took place inside the furnace, and the resultant TiO_2 particles (~35±10 nm in diameter; see transmission electron microscope image in Fig. 1) were carried out of the furnace as an aerosol.

A stainless steel cylindrical chamber (inside diameter 20 cm, height 35 cm) was used to contain the fresh aerosol. At the middle height of the chamber, a curved glass window allowed for light scattering measurements at scattering angles from $\theta = 0° - 120°$.

We take Kn to be the ratio between the mean free path of medium gas (a mixture of air and dry N_2 gas in our experiment) and R_g. Use of R_g is somewhat arbitrary since it is only one of many possible measurers of the aggregate linear dimension. It is also perhaps the simplest and most physical, so we use it. The mean free path for the mixed gas is around 65 nm at ambient temperature and 1 atm of pressure. In the TiO_2 aerosol, $\langle R_g \rangle$ ranges from 500 to 2000 nm. Then Kn under these conditions is between 0.03 and 0.13. In order to expand the Kn range, the chamber pressure was reduced from 1 atm to 1/3, 1/4, 1/6, 1/10, and 1/15 atm of pressure. This increased the mean free path to as much as 975 nm. As a result, Kn was extended over 1.

The colloid investigated consisted of polystyrene spherical particles (uniform Latex microspheres, diameter 28 nm, Duke Scientific Corp.). The starting number density was $\sim 9 \times 10^{11}$ cm^{-3}. NaCl was added to the suspension to induce aggregation with concentration from 0.07 to 0.7 mole in order to cause either reaction limited or diffusion limited cluster aggregation. The Knudsen number in the colloid is much less than 1. Quantifying Kn is somewhat problematic because the concept of mean free path is best described in a rarified gas rather than a dense liquid. We shall somewhat arbitrarily (again) take the mean free path of water molecules as 0.3 nm (the side of a cube that contains on average one water molecule). This will allow us to calculate Kn for our colloids and consider them along side the aerosols. No Kn dependence was observed for the colloidal diffusive transport, and all the calculated Kn is much less than 1 so the precise value of this mean free path is not important.

Both static and dynamic light scattering were performed by employing a vertically polarized Ar ion laser with wavelength $\lambda = 488$ nm. The wave vector range for the SLS experiment was $q = 0.4$–$22\ \mu\mathrm{m}^{-1}$. Dynamic light scattering was carried out by using an ALV5000 digital autocorrelator.

When measuring $\langle R_g \rangle$ and $\langle R_m \rangle$ for both the TiO_2 aerosol and the polystyrene sphere colloid, the DLS and SLS experiments were conducted as follows. First a DLS measurement was completed at one angle θ between 20° and 50° to yield a $\langle R_{m1} \rangle$. This normally took 30 s. Next was a SLS measurement in the Guinier regime (usually a series of angles from $\theta = 3°$ to 20°) to produce a $\langle R_g \rangle$. The SLS measurement took around 100 s. Then, another DLS measurement was carried out to find a $\langle R_{m2} \rangle$. The average of $\langle R_{m1} \rangle$ and $\langle R_{m2} \rangle$ was chosen to be the $\langle R_m \rangle$ corresponding to the $\langle R_g \rangle$ measured in between. Usually, $\langle R_{m1} \rangle$ and $\langle R_{m2} \rangle$ were within 10% of each other for DLCA aggregates. After that, SLS experiments at large scattering angles ($\theta > 20°$) were conducted to determine the fractal dimension. The whole procedure was repeated many times to measure the $\langle R_m \rangle$ and $\langle R_g \rangle$ as a function of Kn, which evolves because the system (either aerosol or colloid) was aggregating.

IV. RESULTS AND DISCUSSION

A. Measurement of the radius of gyration and the mobility radius

Figure 2 shows a selected SLS measurement for a TiO_2 aerosol under one of our most difficult experimental situations, 1/10 atm of pressure. There are five consecutive runs. The clear features of this graph are the following. (1) In the large q region ($q > 5\ \mu\mathrm{m}^{-1}$), the five sets of data roughly overlap. Thus it is clear that the five measurements have essentially the same fractal dimension. The value of the fractal dimension was found to be 1.75±0.1, consistent with previously reported values for the diffusion limited cluster aggregation system [2,3]. (2) The apparent intensity increase in the small q region ($q < 1\ \mu\mathrm{m}^{-1}$) is a clear indication of the Tyndall effect due to aggregation. (3) Since the Tyndall effect occurs only in the Rayleigh regime, it is safe for us to say that the data around $q \sim 1\ \mu\mathrm{m}^{-1}$ are in the Guinier region for our TiO_2 aerosol. By plotting $I(0)/I(q)$ vs q^2 in the Guinier regime (see Fig. 3), $\langle R_g \rangle$ was obtained. Apparently,

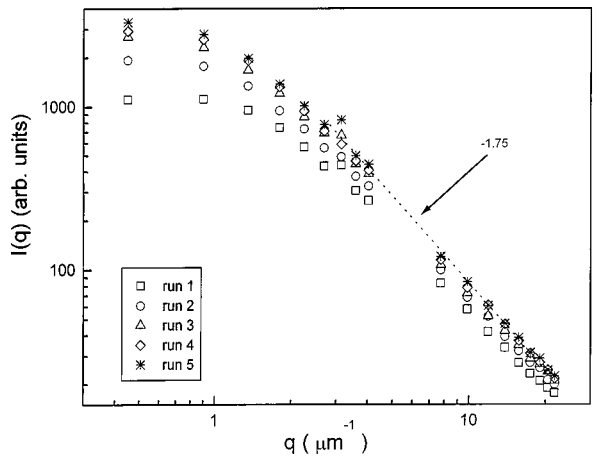

FIG. 2. Scattered intensity measured by SLS as a function of the wave vector q for the TiO_2 aerosol under 1/10 atmospheric pressure. The slope in the large q regime for this log-log plot is the fractal dimension $D_f=1.75$. Five sets of data represent five consecutive runs.

$\langle R_g \rangle$ increases with time due to aggregation. It was noticed during the experiments that the measured intensity fluctuated $\sim 10\%$ over time scales of tenths of a second. We believe these fluctuations are due to the fluctuations in the cluster number density in the focused scattering volume. This caused the measured $\langle R_g \rangle$ to have an uncertainty of $\sim 10\%$.

The corresponding DLS measurements are shown in Fig. 4. The photomultiplier tube (PMT) was placed at a scattering angle of 50° to yield $q=10.9\ \mu m^{-1}$. As can be seen, there are at least two apparent decays in the autocorrelation curves: one in the small time region ($t<0.5$ ms) and another in the larger time region ($t>20$ ms). Analysis shows the first decay to be exponential and related to aggregate diffusive motion, and hence contains τ_c. The second decay has a Gaussian shape and is associated with the number density fluctuations mentioned above. Fittings based on these two components give reasonable fits to the experimental data in these two regimes. However, a misfit is clearly visible in the intermediate regime $1<t<20$ ms, as seen in Fig. 5 where we plot one of the runs in Fig. 4 against the fit. To improve the accuracy of the fitting, a third, *ad hoc* exponential term

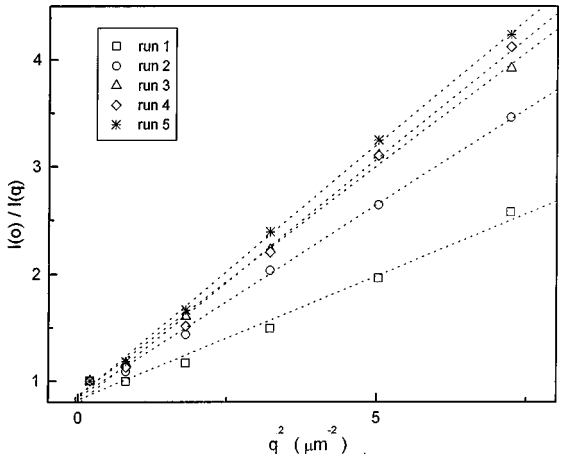

FIG. 3. Guinier analysis of scattering data in Fig. 2. A linear fit yields a slope which is equal to $R_g^2/3$.

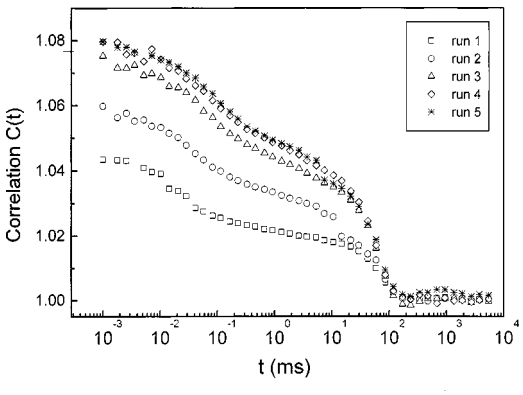

FIG. 4. Scattered light intensity autocorrelation function measured by DLS vs lag time for the TiO_2 aerosol under 1/10 atmospheric pressure.

was added. Hence the scattered light autocorrelation function $C(t)$ was finally fitted by three terms:

$$C(t)=B_0+B_1e^{-t/\tau_c}+B_2e^{-t^2/\tau_2^2}+B_3e^{-t/\tau_3}, \qquad (17)$$

where B_3 and τ_3 are two additional fit variables of the *ad hoc* term. As shown by Fig. 5, this three-term fit matches the experimental data well.

Questions arise from above three-term fit, viz. what does the third term represent and how does it affect τ_c? The third term appears to be related to another diffusive motion; we believe it is due to some extra large clusters in the aerosol. One possible source for these extra large clusters is the TiO_2 deposited on the furnace wall during the thermal decomposition. When the aerosol was carried into the chamber, this furnace wall TiO_2 may have broken off into large clusters. Regardless of the source of this third term, in comparison with the two-term fit, R_m obtained from the three-term fit is generally around 15% smaller, as shown by Fig. 5. This percentage is slightly over the experimental random uncertainty ($\leqslant 10\%$). We believe it is a good and necessary improvement from both mathematical and physical points of view.

Referring back to Fig. 4, we see that as the experiment progressed, the first decay shifted to a larger time. This is the indication of an increase in $\langle R_m \rangle$ due to aggregation, consistent with the SLS measurements. On the other hand, Fig. 4 also shows that the second decay becomes more apparent with time. This is associated with the aggregation process as

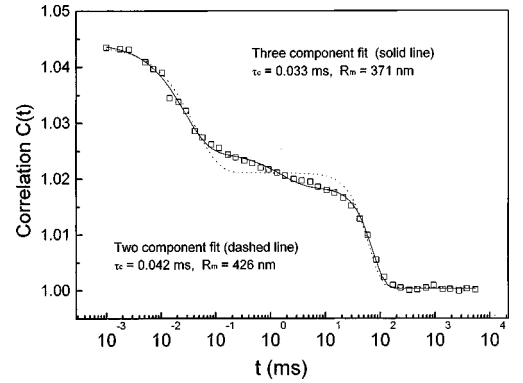

FIG. 5. A selected two and three term fit to the autocorrelation function data in Fig. 4.

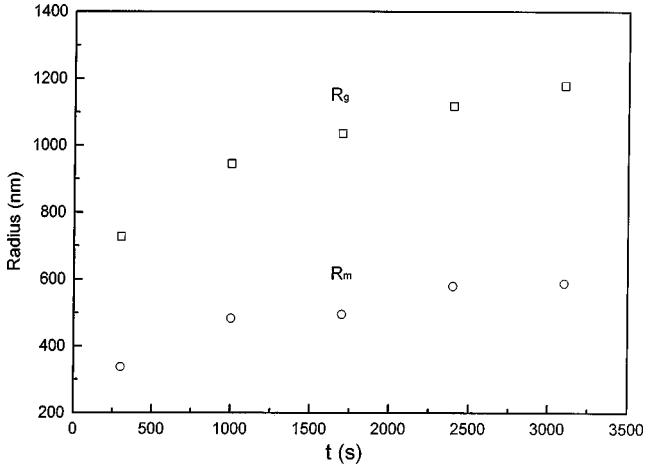

FIG. 6. Time evolution of R_m and R_g for the aerosol under 1/10 atmospheric pressure.

well, since, as the clusters become larger during aggregation, the number density decreases; hence the relative size of the number density fluctuation increases [23].

For many of our aerosols, Kn was quite close to 1, thus Eqs. (13) and (15) should be used to calculate $\langle R_m \rangle$. However, these equations are not easy to invert for $\langle R_m \rangle$. Cai and Sorensen [16,24] showed that, using $D = D_s + D_e$ as the diffusion coefficient throughout the transition regime, where D_s and D_e are the diffusion coefficients for the continuum and free molecular regimes, yields $\langle R_m \rangle$, almost identical to that given by the exact method of using Eqs. (13) and (15). Here we adopt this approach to calculate $\langle R_m \rangle$. The results for both $\langle R_g \rangle$ and $\langle R_m \rangle$ are shown in Fig. 6, where we see that each increases with time.

For the polystyrene sphere colloid with an initial number density of 9×10^{11} cm^{-3}, we observed a diffusion limited cluster aggregation when the NaCl concentration was ~ 0.5 mole or higher. Decreasing the NaCl concentration to ~ 0.07 mole resulted in reaction limited cluster aggregation. The identification of DLCA or RLCA system is based on the measurements of the fractal dimension by SLS and the growth kinetics by DLS. For high NaCl concentrations our optical structure factor measurements found $D_f = 1.75 \pm 0.1$ and a power-law growth of $\langle R_m \rangle$ to imply DLCA, whereas for low NaCl concentration we found $D_f = 2.15 \pm 0.1$ and exponent growth of $\langle R_m \rangle$ to imply RLCA [25–27].

B. Corrections for polydispersity

Ideally, if the aggregates in either an aerosol or a colloid are monodisperse (no aggregate size distribution), $\langle R_m \rangle$ and $\langle R_g \rangle$ can be directly compared because they are associated with same size aggregate. However, the real aggregate systems are polydisperse because of the aggregation process. Due to this size distribution, the measured $\langle R_m \rangle$ and $\langle R_g \rangle$ cannot be directly compared since they represent different moments of the particle size distribution.

To overcome this problem, one can compare $R_{m,0}$ and $R_{g,0}$, since they both are related to the same mean size of the distribution. To calculate $R_{m,0}$ and $R_{g,0}$ for the polydisperse aggregates, we need to know the particle size distribution. Here we will use the scaling distribution, which is known to be produced by the aggregation process [28,29]. Another distribution often used in the aerosol literature is the log normal distribution, but we do not use it here because of the inaccuracies of its higher order moments necessary for the light scattering analysis.

The scaling distribution is given by [21,28,29]

$$n(N) = M_1 s_1^{-2} \phi(x), \tag{18}$$

$$x = N/s_1, \tag{19}$$

$$s_1 = M_1/M_0, \tag{20}$$

$$\phi(x) = A x^{-\tau} e^{-\alpha x}. \tag{21}$$

In Eqs. (18), (19), (20), and (21), s_1 is the mean aggregate size, M_0 and M_1 are the zeroth and first moments of the size distribution, equal to the total number of clusters and monomers, respectively, and A, α, and τ are constants. The ith moment of the size distribution, M_i, is

$$M_i = \int_0^\infty N^i n(N) dN \tag{22}$$

$$= M_1 s_1^{i-1} m_i, \tag{23}$$

where

$$m_i = A \alpha^{-(i+\alpha)} \Gamma(i+\alpha), \tag{24}$$

and where Γ is the gamma function. Normalization leads to $A = \alpha^\alpha \Gamma^{-1}(\alpha)$ and $\alpha = 1 - \tau$. The exponent τ is a measure of the width of the distribution; the larger τ is, the wider the distribution. It is also equal to the aggregation kernel homogeneity for certain classes of kernels including DLCA [29].

To determine how the measured $\langle R_g \rangle$ is related to the moments of the size distribution, we recognize that the measured structure factor $\langle S(q) \rangle$ is an average of the individual aggregate $S(q)$ over the size distribution weighted by the light scattering; hence

$$\langle S(q) \rangle = \frac{\int_0^\infty N^2 n(N) S(q) dN}{\int_0^\infty N^2 n(N) dN}. \tag{25}$$

Since R_g is measured in the Guinier regime, we use Eq. (5) in Eq. (25) to obtain

$$\langle S(q) \rangle = 1 - \tfrac{1}{3} q^2 \langle R_g^2 \rangle, \tag{26}$$

where

$$\langle R_g^2 \rangle = k_0^{-2/D_f} a^2 \frac{M_{2+2/D_f}}{M_2} \tag{27}$$

$$= R_{g,0}^2 \frac{m_{2+2/D_f}}{m_2}. \tag{28}$$

In Eq. (28) we have used $R_{g,0} = k_0^{-1/D_f} a s_1^{1/D_f}$, the radius of gyration of the mean aggregate sizes. Equation (28) allows

the measured $\langle R_g^2 \rangle$ to be converted to $R_{g,o}$, the radius of gyration of the mean size aggregate.

The relation of the mobility radius of a fractal aggregate to N is not as well understood as the radius of gyration, so we assume the more general form of $R_m = aN^x$, which is supported by the experimental measurements [16]. Under this assumption, we can work out the relationship among $\langle R_m \rangle$, the moments of size distribution, and $R_{m,0}$, as we did for the radius of gyration above.

The measured $\langle \tau_c \rangle$ is an average of τ_c over the intensity weighted size distribution; hence

$$\langle \tau_c \rangle = \frac{\int_0^\infty I(N) n(N) \tau_c(N) dN}{\int_0^\infty I(N) n(N) dN}, \tag{29}$$

where $\tau_c(N)$ is the correlation time for a aggregate of N monomers. As described in Sec. II, $I(N) \propto N^2$ in the Rayleigh scattering regime and $I(N) \propto N$ in the power-law scattering regime. On the other hand, $\tau_c(N) \propto R_m$ in the continuum regime and $\tau_c(N) \propto R_m^2$ in the free molecular regime. These conditions applied to Eq. (29) along with the mobility radius of the mean size $R_{m,o} = a s_1^x$ yield for scattering in the Rayleigh regime:

$$\langle R_m \rangle = R_{m,0} \frac{m_2}{m_{2-x}} \quad \text{continuum regime,} \tag{30}$$

$$\langle R_m^2 \rangle = R_{m,0}^2 \frac{m_2}{m_{2-2x}} \quad \text{free molecular regime,} \tag{31}$$

and, for scattering in the power-law regime

$$\langle R_m \rangle = R_{m,0} \frac{m_1}{m_{1-x}} \quad \text{continuum regime,} \tag{32}$$

$$\langle R_m^2 \rangle = R_{m,0}^2 \frac{m_1}{m_{1-2x}} \quad \text{free molecular regime.} \tag{33}$$

Accordingly, the ratio between $R_{m,0}$ and $R_{g,0}$ was calculated based on our measured $\langle R_m \rangle$ and $\langle R_g \rangle$ data for both the aerosol and the colloid. When calculating $R_{m,0}$ and $R_{g,0}$, the following factors have been used to determine the variables and to determine which equations should be used. (1) For the atmospheric pressure aerosol, Kn is far less than 1 (hence in the continuum regime), experiments (e.g., Ref. [16]) and our recent kinetic investigation [30] has shown that the kernel homogeneity is $\tau \simeq 0$; hence $\alpha = 1$, as expected theoretically for this regime. Also, since our measurements show $\langle R_m \rangle$ to be proportional to $\langle R_g \rangle$, x was chosen to be $1/D_f$ ($D_f = 1.75$). On the other hand, for low pressure experiments (e.g., 1/10 and 1/15 atmospheric pressure), the initial Kn is close to 1. Our recent kinetic investigation [30] suggests for this regime $\tau = -1/D_f$. Again, this is consistent with theoretical expectation. Since $\tau = -1/D_f$, $\alpha = 1 + 1/D_f$. Again, $\langle R_m \rangle \propto \langle R_g \rangle$ implies $x = 1/D_f$. (2) For the colloid, $\tau = 1.5$, $\alpha = -0.5$, and $x = 1/D_f$ ($D_f = 2.15$) were used for RLCA according to Refs. [10,26,27], whereas $\tau = 0$, $\alpha = 1$, and $x = 1/D_f$ ($D_f = 1.75$) were adopted for DLCA. Finally, care was taken to use DLS data taken in either the Rayleigh ($qR_g \ll 1$) or power-law ($qR_g \gg 1$) regimes, and Eqs. (30) and (31) or (32) and (33) were used as appropriate.

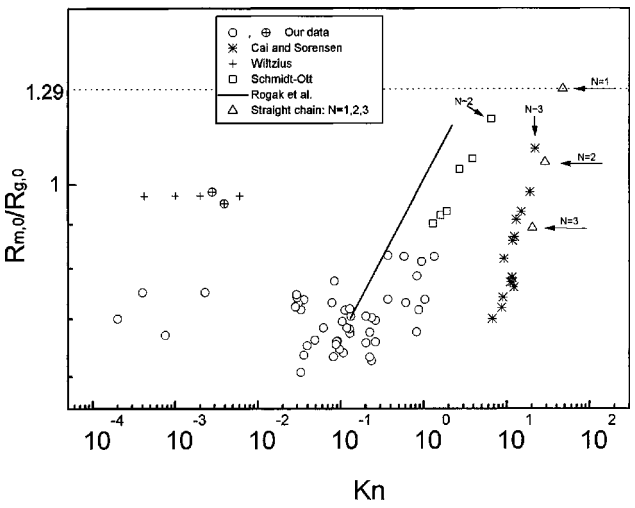

FIG. 7. The ratio of $R_{m,0}/R_{g,0}$ as a function of Knudsen number Kn. Also included are the data of Wiltzius, Schmidt-Ott, Rogak, Flagan, and Nguyen, and Cai and Sorensen, along with the calculated values of R_m/R_g for a straight chain of spheres assuming the single sphere ($N=1$) has a Knudsen number of 47.3 (the mfp is 330 nm, $a=9$ nm, and $R_g=7.0$ nm). The dashed line is at $R_{m,0}/R_{g,0}=1.29$, the $N=1$ sphere limit. The data of Wiltzius and our data of $R_{m,0}/R_{g,0} \simeq 0.97$ are for $D_f \simeq 2.15$, the rest are for $D_f \simeq 1.75$. All data with Kn<0.01 are from a colloid, and all with Kn>0.01 are from an aerosol.

C. R_m/R_g when Kn<1

Figure 7 plots the primary experimental result of this paper: the ratio of $R_{m,0}$ and $R_{g,0}$ as a function of Kn. In comparison, results obtained by Wiltzius [9] and Cai and Sorensen [16] are also included in the graph. Notice that in calculating $R_{m,0}$ and $R_{g,0}$ for Cai and Sorensen's experimental results, $\tau = 0.2$, $\alpha = 0.8$, and $x = 0.43$, were used as reported by them [16]. As can be seen, the ratio between $R_{m,0}$ and $R_{g,0}$ for our TiO_2 aerosol is nearly constant (0.70 ± 0.05) in the Kn range of 0.02–0.3 with a slight increase to 0.75 ± 0.05 for $0.4 <$ Kn < 1.3. For the colloid investigated, Kn $\leqslant 0.004$, the ratio of $R_{m,0}/R_{g,0}$ is 0.71 ± 0.05 for DLCA and 0.97 ± 0.05 for RLCA.

Several conclusions can be made from Fig. 7. First, a constant ratio indicates that $R_{m,0}$ is proportional to $R_{g,0}$ once Kn$\leqslant 1$, regardless of the type of aggregation (RLCA or DLCA) and the system of aggregation (aerosol or colloid). This is a generalization of Wiltzius's conclusion. Second, our data reveal that the ratio of $R_{m,0}$ and $R_{g,0}$ depends strongly on the fractal dimension. This dependence will be addressed below in terms of a hydrodynamic calculation. Third, comparison of our data to those of Cai and Sorensen implies a transition from constant R_m/R_g to one which increases with increasing Kn.

As mentioned above, the ratio between $R_{m,0}$ and $R_{g,0}$ is different for DLCA ($D_f \simeq 1.8$) and RLCA ($D_f \simeq 2.15$). In order to explain this difference, we consider a simple hydrodynamic model [8,9,31]. We assume the monomer pair correlation $g(r)$ has the form of

TABLE I. The calculated ratio between the mobility radius and the radius of gyration using Eq. (35) for three different density autocorrelation function cutoffs as a function of the fractal dimension.

D_f	Exponential cutoff R_m/R_g	Gaussian cutoff R_m/R_g	Step cutoff R_m/R_g
1.5	0.37	0.57	0.72
1.6	0.41	0.62	0.80
1.7	0.46	0.67	0.86
1.8	0.50	0.72	0.91
1.9	0.54	0.76	0.96
2.0	0.58	0.80	1.00
2.1	0.61	0.83	1.03

$$g(r) \propto r^{D_f-3} h(r), \tag{34}$$

where $h(r)$ is the cutoff function. Then for a spherical aggregate with fractal dimension D_f (only one aggregate and no size distribution; hence $R_{m,0}=R_m$ and $R_{g,0}=R_g$), hydrodynamic theory [31] gives

$$\frac{R_m}{R_g} = \frac{\int_0^\infty r^2 g(r)dr}{\int_0^\infty r g(r)dr} \left[\frac{2\int_0^\infty r^2 g(r)dr}{\int_0^\infty r^4 g(r)dr} \right]^{1/2}. \tag{35}$$

The calculated ratios of R_m/R_g are listed in Table I for some commonly used cutoff functions such as the exponential and Gaussian and also for a step cutoff, which is unphysical but demonstrates the sharp cutoff limit.

Given that the TiO_2 aerosol as well as the DLCA colloid have a fractal dimension 1.75 ± 0.1, the model predicts ratios of 0.48, 0.70, and 0.89 if the monomer pair correlation of the aggregates has an exponential, a Gaussian, or a step function cutoff, respectively. The ratio calculated by using a Gaussian cutoff function is essentially the same as the experimentally measured value. Previous work from this lab has used both SLS [32] and electron microscopy imaging [33] and a comprehensive analysis of proposed structure factors [19] to show that the cutoff function is much sharper than exponential and well described by the Gaussian. Thus the theoretical model embodied in Eq. (35) is successful in calculating R_m/R_g.

Equation (35) predicts ratios of 0.63, 0.85, and 1.05 for the RLCA ($D_f=2.15$) aggregates by using an exponential, a Gaussian, and a step function cutoff, respectively. The experimentally measured value of $R_m/R_g=0.97\pm0.05$ is between those calculated using the Gaussian and step function cutoffs. Thus the experimentally measured ratio suggests that the monomer pair correlation of RLCA falls off at the perimeter quicker than a Gaussian cutoff function. Considerably less work has been applied to determining the cutoff of RLCA aggregates than DLCA aggregates. Our recent analysis [19] of the structure factor simulations of Lin *et al.* [34] suggest that the Gaussian describes the cutoff well for RLCA. In that case the prediction of Eq. (35) of $R_m/R_g=0.85\pm0.02$ is in slight disagreement with our experimental value of 0.97 ± 0.05 and the reanalyzed Wiltzius value of 0.98. On the other hand, in a computer simulation carried out by Chen, Meakin, and Deutch [10b], a ratio of $R_m/R_g=0.97$ was reported for RLCA, which agrees well with the experimental results.

Other workers have considered the theoretical problem of drag on a fractal in the continuum regime. Rogak and Flagan [14] created a series of fractal clusters with different D_f based on an iterative ''expanded cube'' procedure. For $D_f=1.79$ they found $R_m/R_g=0.67$, in good agreement with our measurements, and for $D_f=2.1$ and $R_m/R_g\simeq0.73$, in poor agreement with the measurements. Tandon and Rosner [17] calculated the diffusivity for arbitrary D_f. Their graphical results (Fig. 5 of Ref. [17]) can be used to infer R_m/R_g with the application of Eq. (1). With $k_o=1.3$ [4,32], we find $R_m/R_g\simeq0.71$ for $D_f=1.8$, and $R_m/R_g\simeq0.95$ for $D_f=2.18$, both in excellent agreement with the measurements.

D. R_m/R_g when Kn>1

Despite performing experiments at 1/15 of an atmosphere where the mean free path in air is 975 nm, we were unable to exceed Kn=1.3, and thereby probe deeply into the large Kn, free molecular regime. However, by combining our current results with previous data, we can create a description of fractal aggregate mobility for all Kn.

Data for fractal aggregate mobility involving the deepest excursion into the large Kn regime are those of Cai and Sorensen [16], who used both DLS and SLS to measure R_m and R_g for soot fractal aggregates in a flame. They found the ratio was not a constant but rather $R_m/R_g \propto N^{-0.13} \propto R_g^{-0.23}$ with $D_f=1.79\pm0.10$. The exact dependence was found to be $R_m=\beta a N^x$, where a is the monomer radius, also measured *in situ*, $\beta=0.99\pm0.02$, and $x=0.43\pm0.03$. This result was nicely explained as due to the projected area of the aggregate which is effective for momentum transfer between the gas molecules and the aggregate in the kinetic regime, Kn$\gg$1. For $D_f<2$, the cluster is nearly transparent to mean that the projected area should be $\pi a^2 N$, thus $R_m=aN^{1/2}$. The exponent $x=0.43$, less than the expected x=1/2, was explained as due to some small degree of monomer-monomer screening. A comparison was made to screening that also occurs between monomers for electrons in transmission electron microscopy imaging of fractal aggregates from a three-dimensional to a two-dimensional image [34–38]. For TEM imaging it has been found that the projected area goes as $N^{0.87\pm0.05}$. Since electrons in a TEM and the gas molecules in an aerosol when Kn$\gg$1 travel in straight lines, the TEM result implies $R_m \sim N^x$ with $x=0.87/2=0.435$, very consistent with the 0.43 measured. Further support for this dependency was gained from Meakin, Donn, and Mulholland [13] who with computer simulations studied monomer screening in aggregates to imply $x=0.45$. Thus we have an intuitively pleasing physical picture of drag on fractal aggregates when Kn$\gg$1 caused by ballistic bombardment of gas molecules on individual spherical monomers adding linearly, with the exception of some monomer-monomer screening, to give the total drag on the aggregate.

We know of two other significant data sets for mobility of fractal aggregates not in the continuum (Kn$\ll$1) regime. Schmidt-Ott [12] used two electrostatic classifiers to study silver fractal aggregates with monomer size of $a=7.5$ nm.

The aggregate aerosol passed through the first analyzer and the mobility radius was measured for the ramified aggregates. The aerosol then passed through a furnace which sintered the aggregates into dense spheres. The second analyzer measured the dense sphere radius R. It was found that $R_m \sim R^{1.375}$. Since $N \sim R^3$, it can be inferred that $N \sim R_m^{2.18}$. Schmidt-Ott interpreted this as the fractal dimension, but this holds only if R_m/R_g is constant, which may not be true for $\mathrm{Kn} \gg 1$.

We have reanalyzed Schmidt-Ott's data. The number of monomers per cluster before sintering can be determined from the measured R and a and $N=(R/a)^3$. We assume $D_f = 1.75$, which is well known and verified for aggregates formed by random diffusion (DLCA) like Schmidt-Ott's. Then Eq. (1) with $k_0 = 1.3$ yields R_g. We now can plot R_m/R_g vs Kn with a mean free path of 65 nm for room temperature air in Fig. 7. The dependency in Fig. 7 is described by $R_m/R_g \sim \mathrm{Kn}^{0.19}$, which for $D_f = 1.75$ is equivalent to $R_m \sim N^{0.46}$. This is consistent with Cai and Sorensen, and the similarity of slopes in Fig. 7 testifies to this similarity.

Rogak, Flagan, and Nguyen [15] also used electrostatic classifiers to measure aggregate mobility and size before and after sintering. Both TiO_2 and Si aerosols were used. They found $R_m \sim R_g^{D_\beta/2}$, where $D_\beta = 1.59 \pm 0.04$ represented a ''mobility fractal dimension.'' Here again we reinterpret their data based on the most probable fact that their aggregates, formed by random diffusion, are DLCA aggregates with $D_f \simeq 1.75$. Then the result above implies $R_m/R_g \sim R_g^{-0.205} \sim N^{-0.12}$, not a constant, and thus $R_m \sim N^{0.45}$. Once again consistency is found, now with both Cai and Sorensen and Schmidt-Ott. In Fig. 7 we include the result of Rogak, Flagan, and Nguyen, as their best fit line from their Fig. 13.

The corroboration of the three data sets above to imply that $R_m \sim N^{0.45}$ is deceptive, and the deception is enhanced given the agreement with the theoretical explanation given above. The deception lies in the fact that not all the data lie in the large Kn regime where the kinetic explanation applies. Indeed, the data of Ref. [15], are for $0.13 \leqslant \mathrm{Kn} \leqslant 2.2$, a range definitely not in the free molecular limit. Why do our aerosol data show a constant $R_m/R_g = 0.75 \pm 0.05$, whereas the data of Ref. [15] vary greatly in the same Kn range? Further, what is the source of variation of R_m/R_g for all three data sets?

The answer partially lies in the number of monomers per aggregate and the single particle limit. Included in Fig. 7 are values of N for some of the data points for each data set. The smallest N values are $\sim 2-3$ in each case. Consider the $N=1$ limit, a single sphere, then $R_m = R$, and $R_g = \sqrt{3/5}R$, hence $R_m/R_g = 1.29$. This limit is included in Fig. 7 as a dashed line, and the obvious implication is that each data set is approaching its single particle ($N=1$) limit regardless of Kn. Chan and Dahneke [6] calculated the free molecular regime R_m for straight chains of spheres of arbitrary N. They found

$$R_m = a\sqrt{0.802(N-1)+1}. \tag{36}$$

In Fig. 7 we include their results with Kn adjusted to match approximately with the data of Cai and Sorensen. The comparison is quite good for $N=2$ and 3, but deteriorates for larger N because fractal aggregates are poorly described by straight chains when N is larger than a few.

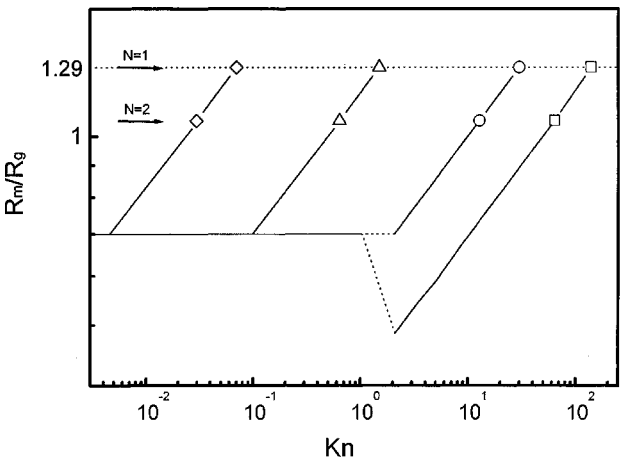

FIG. 8. A schematic diagram for the ratio R_m/R_g of a fractal aggregate with $D_f = 1.75$ as a function of the Knudsen number Kn which is equal to the mean free path of the medium molecules divided by R_g. Examples for various initial, $N=1$ and 2, Knudsen numbers are shown. For a given monomer size the gas molecule mean free path establishes a monomer Knudsen number for which $R_m/R_g = 1.29$. As the number of monomers in the aggregate N increases, Kn decreases, and R_m/R_g follows the drawn curves which are dependent upon the initial, monomer Knudsen number.

We can now make an assessment of Fig. 7. The data of Ref. [15] are centered on $\mathrm{Kn} \simeq 1$; hence kinetic theory, which predicts $R_m \sim N^{0.45}$, may only marginally apply. The fact that the data agree with this is as much coincidence as an endorsement of the kinetic theory that predicts $R_m = aN^{0.45}$. The coincidence is caused by the need for R_m/R_g to rise up from 0.75, the large N limit when $\mathrm{Kn} \simeq 1$, to 1.29 as $N \to 1$. The data of Cai and Sorensen for which $6.7 \leqslant \mathrm{Kn} \leqslant 22$ are well in the free molecular regime where the kinetic theory applies, hence the agreement of data and theory is confirmation of theory. Schmidt-Ott's data lie between these two data sets with $1.3 \leqslant \mathrm{Kn} \leqslant 6.5$, and probably reflect portions of each argument. All three data sets have the correct small N limit, which they must.

Finally, we put all of this together in a coherent description of R_m for fractal aggregates which is depicted in Fig. 8. For large Kn we adhere to the result of Cai and Sorensen that

$$R_m = aN^x, \tag{37}$$

with $x = 0.44 \pm 0.03$ for $D_f \simeq 1.75$. This value of the exponent x is based on all three data sets in Fig. 7, the results of Ref. [13], and the electron microscope screening results [35–38]. Remarkably, and gratifyingly, Eqs. (36), the Chan and Dahneke result for straight chains, and Eq. (37) agree to better than 1% for $N=1-4$. Therefore, we claim that Eq. (37) holds for all $N \geqslant 1$. When Eq. (37) is combined with Eq. (1), we find the ratio

$$R_m/R_g = k_o^{1/D_f} N^{x-1/D_f}. \tag{38}$$

Furthermore, since we have defined the aggregate Knudsen number as the ratio of the gas molecule mean free path to the aggregate radius of gyration, Eq. (38) implies

$$R_m/R_g \propto Kn^{1-xD_f}. \tag{39}$$

As the Knudsen number falls with increasing N, the behavior of R_m must cross over from Eqs. (38) and (39) to the continuum behavior, $R_m = 0.7R_g$. However, the manner in which this occurs depends upon the Knudsen number of the monomers of the aggregate. If this monomer Knudsen number is sufficiently large, the Kn dependency in Eq. (39), which for $D_f = 1.75$ is $\mathrm{Kn}^{0.23}$, can lead the ratio R_m/R_g to values less than the continuum value of 0.7 while Kn is still greater than 1. However, as Kn continues to fall into the continum regime this undershoot of R_m/R_g, as sketched in Fig. 8, must be rectified, in some unknown manner, to $R_m/R_g = 0.7$. This unknown rectification is represented by the dashed line in Fig. 8. On the other hand, smaller values of the monomer Knudsen number (approximation those which are less than 15) will lead to a value of R_m/R_g declining monotonically from 1.29 to 0.7 as the aggregate Knudsen number falls. Such a behavior is also sketched in Fig. 8.

One surprising result of our work here is that R_m/R_g must decrease from a monomer value of 1.29 to the ''large cluster'' value of 0.7 regardless of the value of Kn. When Kn is large, Eq. (37) with $x = 0.44$ describes this decrease as described above. When $\mathrm{Kn} \leqslant 1$, a form similar to Eq. (37) may hold, but the exponent x for this regime has yet to be determined. This behavior is also sketched in Fig. 8.

V. CONCLUSIONS

Static and dynamic light scattering were used to determine fractal aggregate radius of gyration, fractal dimension, and mobility radius in aerosols and colloids for both DLCA ($D_f \simeq 1.75$) and RLCA ($D_f \simeq 2.15$) aggregates. In the continuum limit ($\mathrm{Kn} \simeq 0$) $R_m/R_g = 0.70 \pm 0.05$ for $D_f \simeq 1.75$ and $R_m/R_g = 0.97 \pm 0.05$ for $D_f \simeq 2.15$. These ratios were independent of whether the system was an aerosol or a colloid and in agreement with theory for aggregates with density correlation functions sharply cutoff like a Gaussian. For $\mathrm{Kn} \leqslant 1.3$ and $D_f = 1.75$, the ratio R_m/R_g remains fairly constant increasing, within error, to 0.75 ± 0.05 at $\mathrm{Kn} = 1.3$. These results apply for $N \gg 1$, but as $N \to 1$ the single particle limit $R_m/R_g = 1.29$ must be approached. The free molecular limit was studied with use of previous data, some reanalyzed, to find $R_m = aN^{0.44 \pm 0.03}$ when $\mathrm{Kn} > 1$. This formula has the correct $N \to 1$ limit. In this regime $R_m/R_g \sim N^{-(0.13 \pm 0.03)}$ for $D_f \simeq 1.75$, not a constant. Figure 8 gives a schematic description of R_m/R_g for all Kn when Kn is varied via N. A discussion of Fig. 8 is given immediately above the conclusion.

ACKNOWLEDGEMENT

This research was supported by the National Science Foundation under Grant No. CTS 9709764.

[1] S.R. Forrest and T.A. Witten, Jr., J. Phys. A **12**, L109 (1979).
[2] *Kinetics of Aggregation and Gelation*, edited by F. Family and D. P. Landau (North-Holland, Amsterdam, 1984).
[3] R. Jullien and R. Botet, *Aggregation and Fractal Aggregates* (World Scientific, Singapore, 1987).
[4] C.M. Sorensen and G.C. Roberts, J. Colloid Interface Sci. **186**, 447 (1997).
[5] J.F. van de Vate, W.F. van Leeuwen, A. Plomp, and H.C.D. Smit, J. Aerosol Sci. **11**, 67 (1980).
[6] P. Chan and B. Dahneke, J. Appl. Phys. **52**, 3106 (1981).
[7] Z.-Y. Chen, J.M. Deutch, and P. Meakin, J. Chem. Phys. **80**, 2982 (1984).
[8] P. Meakin, Z.-Y. Chen, and J.M. Deutch, J. Chem. Phys. **82**, 3486 (1985).
[9] P. Wiltzius, Phys. Rev. Lett. **58**, 710 (1987).
[10] (a) P.N. Pusey, J.G. Rarity, R. Klein, and D.A. Weitz, Phys. Rev. Lett. **59**, 2122 (1987); (b)Z.-Y. Chen, P. Meakin, and J. M. Deutch, *ibid.* **59**, 2121 (1987).
[11] Z.-Y. Chen, P.C. Weakliem, and P. Meakin, J. Chem. Phys. **89**, 5587 (1988).
[12] A. Schmidt-Ott, Appl. Phys. Lett. **52**, 954 (1988).
[13] P. Meakin, B. Donn, and G.W. Mulholland, Langmuir **5**, 510 (1989).
[14] S.N. Rogak and R.C. Flagan, J. Colloid Interface Sci. **134**, 206 (1990).
[15] S.N. Rogak, R.C. Flagan, and H.V. Nguyen, Aerosol. Sci. Technol. **18**, 25 (1993).
[16] J. Cai and C.M. Sorensen, Phys. Rev. E **50**, 3397 (1994).
[17] P. Tandon and D.E. Rosner, Ind. Eng. Chem. Res. **34**, 3265 (1995).
[18] C.M. Sorensen, in *Handbook of Surface and Colloid Chemistry*, edited by K.S. Birdi (CRC Press, Boca Raton, FL, 1997).
[19] C.M. Sorensen and G.M. Wang (unpublished).
[20] B. Berne and R. Pecora, *Dynamic Light Scattering* (Wiley, New York, 1976).
[21] S.K. Friedlander, *Smoke, Dust and Haze* (Wiley, New York, 1977).
[22] K. Okuyama, Y. Kousaka, N. Tohge, S. Yamamoto, J.J. Wu, R.C. Flagan, and J.H. Seinfeld, AIChE. J. **32**, 2010 (1986).
[23] D.W. Schaefer and B.J. Berne, Phys. Rev. Lett. **28**, 475 (1972).
[24] J. Cai, Ph. D dissertation, Kansas State University, 1994.
[25] R.C. Ball, D.A. Weitz, T.A. Witten, and F. Leyvraz, Phys. Rev. Lett. **58**, 274 (1985).
[26] D.A. Weitz and M.Y. Lin, Phys. Rev. Lett. **57**, 2037 (1986).
[27] M.Y. Lin, H.M. Lindsay, D.A. Weitz, R.C. Ball, R. Klein, and P. Meakin, Phys. Rev. A **41**, 2005 (1990).
[28] S.K. Friedlander and C.S. Wang, J. Colloid Interface Sci. **22**, 126 (1966).
[29] P.G.J. van Dongen and M.H. Ernst, Phys. Rev. Lett. **54**, 1396 (1985).
[30] G.M. Wang and C.M. Sorensen (unpublished).
[31] J.G. Kirkwood and J. Riseman, J. Chem. Phys. **16**, 565 (1948).
[32] C.M. Sorensen, J. Cai, and N. Lu, Langmuir **8**, 2064 (1992).
[33] J. Cai, N. Lu, and C.M. Sorensen, J. Colloid Interface Sci. **171**, 470 (1995).
[34] M.Y. Lin, R. Klein, H.M. Lindsay, D.A. Weitz, R.C. Ball, and P. Meakin, J. Colloid Interface Sci. **137**, 263 (1990).
[35] R.J. Samson, G.W. Mulholland, and J.W. Gentry, Langmuir **3**, 272 (1987).
[36] A.I. Medalia and F.A. Heckman, J. Colloid Interface Sci. **4**, 393 (1967); **36**, 173 (1971).
[37] U.O. Koylu and G.M. Faeth, Combust. Flame **89**, 140 (1992).
[38] C. Oh and C.M. Sorensen, J. Colloid Interface Sci. **193**, 17 (1997).